UPDATE OF THE FRENCH AERIAL SURVEY INDEX OF ABUNDANCE AND FIRST ATTEMPT AT INTEGRATING BLUEFIN TUNA SCHOOL SIZE ESTIMATES FROM VIDEO CAMERAS

T. Rouyer[1], B. Brisset[1], Y. Tremblay[1], J.-M. Fromentin[1]

SUMMARY

The French aerial survey provide an important fisheries independent index for the stock assessment of Eastern Atlantic Bluefin Tuna (EABFT, Thunnus thynnus*). However, this survey presents several shortcomings. The main issue is linked to the absence of quantitative estimate of the size of the different school types encountered during the survey. This prevents from accounting to changes in school size composition, which could affect the trends of the index. Since 2016 video cameras were set-up under the aircraft to record the flights and obtain school size estimates. In addition to the 2017 update of the index, the present manuscript describes the procedure to estimate school size from the videos and presents preliminary results for an index integrating this new information. Robustness to school type assignment and school size variability are investigated through bootstrap approaches. The results show distinct surfaces for the different school types and that including school sizes into the index leads to a comparable long-term trend, but with higher values for 2009-2012 than without including the school surfaces.*

RÉSUMÉ

Les prospections aériennes françaises fournissent un important indice indépendant des pêcheries pour l'évaluation du stock de thon rouge de l'Atlantique Est (EABFT, Thunnus thynnus*). Cependant, ces prospections présentent plusieurs lacunes. Le principal problème est lié à l'absence d'estimation quantitative de la taille des différents types de bancs observés au cours de la prospection. Cela empêche de prendre en compte les changements de la composition par taille des bancs, ce qui pourrait affecter les tendances de l'indice. Depuis 2016, des caméras vidéo ont été installées sous l'avion pour filmer les vols et obtenir une estimation de la taille du banc. Outre la mise à jour de l'indice de 2017, le présent document décrit la procédure d'estimation de la taille des bancs à partir des enregistrements vidéo et présente les résultats préliminaires d'un indice intégrant ces nouvelles informations. La robustesse vis-à-vis de l'attribution d'un type de banc et la variabilité de la taille du banc sont étudiées au moyen d'approches de type bootstrap. Les résultats font apparaître diverses surfaces pour les différents types de bancs et montrent que l'inclusion de la taille des bancs dans l'indice aboutit à une tendance comparable à long terme, mais avec des valeurs plus élevées pour 2009-2012 que lorsque la surface des bancs n'est pas incluse.*

RESUMEN

La prospección aérea francesa proporciona un importante índice independiente de la pesquería para la evaluación del stock de atún rojo del Atlántico oriental (EABFT, Thunnus thynnus). *Sin embargo, esta prospección presenta diversas deficiencias. El principal problema está relacionado con la falta una estimación cuantitativa del tamaño de los diferentes tipos de bancos hallados durante la prospección. Esto impide tener en cuenta los cambios en la composición por tallas del banco, lo que podría afectar a las tendencias del índice. Desde 2016, se colocaron cámaras de vídeo bajo la aeronave para grabar los vuelos y obtener estimaciones del tamaño de los bancos. Además de la actualización del índice de 2017, el presente documento describe el procedimiento para estimar el tamaño de los bancos a partir de los vídeos y presenta resultados preliminares para un índice que integre esta nueva*

1. MARBEC Univ Montpellier, CNRS, Ifremer, IRD, Sète, France. Tristan.rouyer@ifremer.fr

información. Se investiga la robustez ante la asignación al tipo de banco y la variabilidad en el tamaño del banco mediante enfoques de bootstrap. Los resultados demuestran superficies diferentes para los distintos tipos de bancos y que incluir el tamaño del banco en el índice conduce a una tendencia a largo plazo comparable, pero con valores más elevados para 2009-2012 que sin incluir las superficies de los bancos.

KEYWORDS

Juvenile Atlantic bluefin tuna, Northwest Mediterranean,
Fisheries independent abundance index, Aerial survey, School size estimate, Video cameras

1. Introduction

The French aerial survey index has been integrated for the first time in the base case VPA of the Eastern Atlantic bluefin tuna (EABFT, *Thunnus thynnus*) stock assessment in 2017. This index is important for the stock assessment. It is one of the two fisheries-independent index included in the stock assessment. The index started in 2000 and has been updated yearly since then, with the exception of 2004-2008. It also covers young fishes from the northeast Mediterranean Sea, for which information is scarce, particularly since the enforcement of the recovery plan limiting the catch of fish below 30kg. Therefore, even if the geographical coverage of juvenile areas is not complete as it only covers the Gulf of Lions (GoL), it provides insights into stock dynamics that cannot be captured by indices covering adults.

This index still has several shortcomings. It does not cover all juveniles areas, among them the Bay of Biscay and the Adriatic. It also does not include effects about detectability related to the position of tuna in the water column, or related to the emigration/immigration in the GoL associated to food availability and changes in oceanographic conditions. However, the main issue is that the survey relies upon the census of EABFT schools feeding at the surface into qualitative size classes. It is therefore not possible to estimate the absolute or the relative size of schools. This is an important issue as changes in school type composition from one year to another will not be accounted for by the index. For instance, years with more numerous small schools will translate into a higher index than years with less numerous but larger schools, even though the total amount of tunas might be higher for the latter. During the 2017 EABFT stock assessment, this issue resulted in the decision to split the French aerial survey into two parts as changes in school size composition has been detected.

To tackle this problem, since 2016 video cameras were installed underneath the wings of the aircraft used for the survey. This system was designed to record the flights and the tuna schools detections that were made under the plane. As the altitude of the flights is constant, this enables to use the videos to estimate the surface of each school type. Doing so, it becomes then possible to quantitatively account for different school sizes in the index of abundance built from this survey. The present paper presents (i) an update of the index of abundance through to 2017, (ii) the methodology developed to achieve such quantification of EABFT school surfaces from video cameras, (iii) preliminary results about integrating it into the index of abundance and (iv) an analysis of the robustness to observation error due to mis-determination of school type.

2. Materials and method

2.1 Reminder of the French aerial survey protocol

The protocol of the French aerial surveys has been described in details into several papers (Fromentin *et al.*, 2003; Bonhommeau *et al.*, 2010; Bauer *et al.*, 2015; Rouyer *et al.*, 2018). It is just provided here as a reminder. Aerial surveys have been carried out since 2000, excepted in 2004-2008 due to a lack of funding. The survey takes place from early-August to mid-October over the Northwestern Mediterranean Sea, in the Gulf of Lions. This period and location is favourable to school detections as EABFT are at the surface in relation to feeding and/or foraging activity.

Depending on weather conditions, up to 20 flights per year were conducted onboard a Cessna C skymaster 337 “push pull” aircraft at 1000 feet above sea level. One pilot and up to three scientists could embark on this aircraft. From 2012 to 2013 a larger plane, a Cessna Caravan 208 ISR, allowed for an IT and video specialist as well as two scientists. Greater flight times were possible, enabling to fly over the whole Gulf of Lions within one

day against two with the Cessna skymaster 337. The plane was flying higher, 1500ft, and a high resolution, gyro-stabilized video-camera allowed to record the flight and to obtain accurate geolocation and images for specific school detections.

The aerial surveys take place around noon when the sun is at its highest to limit sun reflection on the sea for better detection conditions for the observers. To obtain optimal spotting conditions, flights are constrained to specific weather, sunny sky and low wind speed (<10nm/h), to avoid confusion between schools and whitecaps. Four different routes were defined for the surveys (Figure 1), which were comparable in length 667, 648, 580, and 700 km for route 1-4 respectively. The inter-transect distance of 13.8 km reduces chances of double counting schools on subsequent transect line. The aircraft flies at the constant speed of about 200 km/h and these routes can be then flown in less than 5 hours including distance between airport and transect. Initially, for each flight, the route was randomly selected. However, practical constraints such as weather conditions often interfer in that process. The transect sections with unsuitable conditions (clouds and/or breaking waves) were skipped. When the route could not be selected randomly, special attention was paid to maximizing the spatial coverage of the area and to evening out the amount of times the different routes were flown.

Tuna schools were spotted by 1 to 3 trained scientific observers, from both sides of the plane/transects. While these teams changed over time, an overlapping period always allowed for the new members of the team to get appropriately trained to ensure the standardization of school types attribution. A GPS was used to record the position of the plane and detected tuna schools. Each detected school was then attributed to a type “tiny”, “small”, “medium”, “large” or “aggregation” for high concentrations of schools. The spotting conditions such as the wind strength (beaufort scale) and the number of observers onboard were recorded. During the early years, when the density of school was low, perpendicular distances from the plane were initially estimated by taking the GPS position of the school location. However, as the density of schools detected increased over time, it became impossible for the plane to move above the location of each school to take its GPS position. Therefore distances estimates were then realized using marks on the arms supporting the wings, which were set-up to represent pre-defined ground distances (200, 400, 800, 1200, 1800 and 3600m) at the altitude of 300m.

2.2 Density estimate

The analysis of the aerial survey data was based on the distance sampling theory (Buckland *et al.*, 2005; Thomas *et al.*, 2006). In the distance sampling theory the transects, here the routes, are defined within a given area, here the Gulf of Lions. The object of interest, here a tuna school, is recorded along the route, which is surveyed several times during a given period. The theory allows that some, perhaps many, of the objects remain undetected and that variation in detection due to environment or observer could occur, as soon as n, L and w are accurately measured. According to the line transect theory, w is estimated through a detection function, which is a model fitted to the histogram of the perpendicular distances of the detections.

The line transect approach aims to estimate the detection probability per distance (detectability P) and thus to calculate the percentage of sighted and non-sighted objects. The density estimate is given by:

$$\widehat{D_i} = \frac{n_i}{2\,w\,L\,P}$$

The detectability P, also known as observability or sightability, is obtained by fitting a ‘detection function’ to the histogram of distances. It allows to account for other variables, such as school type or environmental conditions (e.g. wind). The shape of the detection function generally is a monotonically decreasing curve, showing a shoulder under which detection remains almost certain and is unaffected by other variables. Here, for this exercise, the hazard rate detection function was fitted to account for differences in detectability linked to the size categories of the schools. However, other effects such as the season of the flight (month), the number of observers onboard and the wind strength (beaufort scale) are important factors that have been shown to affect detectability. They will have to be included in further analyses. Nonetheless, similarly to what was done for the 2017 assessment, they were included for the simple update of the index through to 2017.

The mean density, $\overline{D}$, from r replicates is estimated as follows:

$$\overline{D} = \frac{1}{r}\sum_{i=1}^{i=r} \widehat{D_i}$$

The variance between replicates is estimated as:

$$Var(D) = \frac{1}{r(r-1)} \sum_{i=1}^{i=n} (\widehat{D_i} - \overline{D})^2$$

Time series of densities were computed for each model using an Horvitz-Thomson-like estimator for groups (i.e. clustered population), implemented in the R package *Distance* (Miller *et al.*, 2017). This allowed to compute a density of clusters (i.e. schools) and a density of individuals depending on the cluster size, thus accounting for school surface estimates

2.3 Data acquisition through video cameras and image processing

Initially, one video camera (GOPRO Hero 4, silver) was set-up below each wing of the aircraft, pointing vertically to the ground. After the initial tests, only one camera was kept under the right wing of the plane. The cameras were attached using succion cups (**Figure 2**). Extra batteries were used to ensure the energy autonomy during the flights and 64GB mini SD cards allowed to record ¾ of the flight when shooting in high resolution (4K) and the entire flight when shooting in 1920x1080. Visual observations, GPS waypoints and videos were synchronized so that videos detection events would be easier to find on the videos and to double check detections.

The videos covered more than 20 flights of about 4 hours each. For this first attempt at estimating school size, the entire amount of videos could not be checked. Therefore some flights were selected so that the whole range of different school types, “tiny”, “small”, “medium”, “large” or “aggregation” could be captured by the cameras (**Figure 3**). Unfortunately, aggregations have only been spotted in 2009-2012 and never since then. In addition, differences still need to be made between aggregations that represent one massive surface and those that represent a collection of smaller size schools. They were then excluded from the present analysis. The videos were visualized and a picture was extracted for each tuna school detection.

Simple image processing techniques were used to estimate the school surfaces (**Figure 4**). First the image was transformed into grayscale and normalized to remove saturation effects. The background of the image was then removed with a median filter, which removed most of the sun reflection. A threshold was then applied to the remaining features, which were then suitable for analysis. The location of the school was extracted and an ellipse was fitted to it. The surface of the ellipse was then computed and provided an estimate for the surface of the school. The conversion from pixels to meters was achieved by filming an object whose size was known from 300m away with the camera on the same settings as during the survey. The libraries Imager and conicfit from the statistical software R were used.

2.4 Robustness analysis

When attributing school types to detections, one source of error lies in different observers that diverge in school type attribution, i.e. who attribute a same school to different school types. For the French aerial survey, within one year, this is controlled by randomly cross checking school type attribution between observers. However, there is still a possibility to observe changes in school type attribution across years. If that was not expected to affect the index of abundance when only accounting for school numbers, it has potential to be problematic when accounting for school sizes.

To assess the effect of this type of error on the index, the following procedure was followed. The schools detected further than 1800m away from the plane, half the maximum distance considered during the surveys, were considered prone to error. Among these schools, it was considered that 10% of them could be wrongly attributed to a larger school type and 5% of the remaining could be attributed to a smaller school type. These percentages were arbitrarily attributed, but from field experience it was believed more likely to attribute a larger school size than a smaller. The distributions of school sizes for each school types were then bootstrapped to attribute school size to each school type. The procedure was set-up to avoid sampling the same schools for the movement towards a larger school type and a smaller school type. For the 1000 bootstraps the detection curve was then fitted and the abundance estimated with this procedure.

3. Results

3.1 Distribution of estimated surfaces for the different school types

Fitting ellipses on schools images did not prove complex, but was sometimes affected by the sun glare, which caused white patches. In particular this affected the fit for the large schools as they occupied a large surface of the picture and couldn't be clearly separated from the sun. However, the ellipses fitted reflected the size of the schools.

Although for this preliminary study the sample sizes were low (Table 1), the histogram of the surfaces estimated from the different school types detected seem to displayed separated modes, which was confirmed by the boxplot that displayed little overlap between school types (Fig. 5). A T-test performed on the log-transformed surface data showed that school types explained 81% of variance and that the average surface of the different school types were significantly different between each type ($p<0.001$ for all school types). Investigating the residuals did not show any strong departure from a normal distribution.

The surface of tiny schools ranged between 2 m^2 and 54 m^2, their average length (i.e. average length of estimated main axes) was 3 m. The surface of small schools ranged between 9 m^2 and 743 m^2, their average length was 10 m. The surface of medium schools ranged between 627 m^2 and 1929 m^2, their average length was 23. The surface of large schools ranged between 59490 m^2 and 73536 m^2, their average length was 132m.

3.2 Including school surfaces in to the index and robustness analysis, update of the index for 2017

The updated index of abundance for 2017, which did thus not include school surfaces, displayed a general increasing trend (**Figure 6**). The year 2017 displayed a sharp decrease in density compared to 2016, at a similar level to the 2014 density. The estimates of school surfaces were then used to recompute the index of abundance and the effect of mis-attributing school types was tested. The 1000 runs displayed variability, but the overall trend remained the same over the bootstraps, suggesting that the index obtained was robust to errors in school type attribution. The time series for the abundance index obtained displayed a long-term increasing trend over the whole time period, with 2016 and 2017 being the two highest densities (**Figure 6**). Compared to the index including the school surfaces, the main difference was that the 2009-2012 period was relatively higher compared to 2014 and 2015. The year 2017 also appeared much more important than in the updated index, and was also greater than 2016. This was likely to be due to a large amount of Large school types spotted during the 2017 survey compared to other years.

4. Discussion

The present manuscript present for the first time an objective approach to estimate EABFT school surfaces during the aerial surveys. Traditional approaches to estimate school sizes rely -in the best cases- upon the expertise of professional tuna spotters, which are complex to experimentally validate and inter-calibrate between spotters. The approach used here allows to circumvent errors and/or inter-calibration issues between spotters/years. It provides an objective way of improving the index of abundance derived from the French aerial survey.

Our results suggest that the school types used in the survey are sensible, as the size of EABFT schools were found to be statistically different between them. This is interesting for further work in understanding the underlying reasons for potentially emerging school sizes distinct distributions. However, the data analyzed here for school size estimate has a small sample size and does not accurately represent inter-annual variations as only two years of data were available. The analysis of the complete available dataset and further data acquisition is likely to bring more insights into this aspect.

The update through to 2017 of the French aerial survey index displayed a decrease in 2017. This was counter-intuitive as a large number of schools was detected this year, second to 2016 in total number. Attempt to modify the detection function by excluding the wind or the number of observers from the fit showed that it affected the index. Removing these effects increased the density for 2017, placing it second to 2016. This suggests that the effects accounted for by the detection function should be revised in the future.

The index obtained by integrating the school surfaces into the distance approach, using the R distance package, showed a similar long-term increase than the updated index stock assessment. The main difference observed was that 2014-2015 were not anymore above the 2009-2012 period. This was due to a higher number of large schools during this period compared to 2014-2015, which was composed by more tiny and small schools. The bootstrap approach suggested that the index obtained was also robust to mis-attribution of school types, as this trend did not substantially change when a percentage of schools far from the plane was attributed to a different school type. This was reinsuring about the capacity of the index to provide consistent results. In the present approach, the probabilities of mis-attribution were arbitrary fixed, but this could be improved by estimating it from the overlap between the surface distributions between school types. Once again, a more complete dataset may provide more insights into this aspect.

Another important aspect is that the detection curve fitted to the detection data through the distance package only included the school type effect for this preliminary analysis, i.e. it only accounted for changes in detection probability linked to the school size and did not include the effect of the spotting team, weather conditions etc., as was done for the 2017 stock assessment. This has only been included for the update of the index. They will have to be included and/or revised for a definitive version of the index. Last but not the least, in the present analysis, very large schools were discarded from the analysis, because they were not spotted during the data acquisition. These will need to be used for a definitive index including school surface. In the database, two types of very large schools have been spotted in the GoL. The first category is a high collection of a collection of smaller school types; the second is one large dense surface of EABFT. These two cases can be analyzed within the same framework as for the second category of 'very large school' GPS points delimiting the perimeter of the school are available to estimate the surface. Overall this method looks promising to provide a robust index of abundance for the next stock assessment.

As stressed throughout this manuscript, the analysis performed was preliminary and numerous aspects are to improved. Besides analysing the whole database to increase sample size and representativity, the distortion induced by the lens used on the cameras affect the size of distance estimates depending on where they appear on the picture. Greater distortion occurs at the edge of the pictures captures by the camera. The variability of locations at which the schools were shot on the camera screen allow to partially make up for this by inducing variability in school size estimate and could explain part of the overlap between the tiny and small categories. Also, the conversion from pixel size to meters was done by taking pictures of a known object placed 300m away, equivalent to the plane altitude. However, the altitude is never completely stable and accounting for changes in altitude through the log of the GPS track could also allow for controlling such an effect and improve the final conversion.

The present approach has interesting perspectives to control other aspects of the survey. For instance, one of the main hypotheses for applying the distance approach is a 100% coverage under the plane. This could be controlled using a video approach and would also allow to estimate the percentage of schools missed by spotters depending on their size, as well as errors in distance estimates. These could then be fed into the abundance index to increase its robustness. Finally, using high resolution cameras is under trial to improve school size estimates and get a better understanding of school dynamics. This would enable for using machine learning techniques to automatically detect EABFT schools captures by the cameras. Nonetheless, these techniques are still limited in that they are constrained to analysing the surface. A next substantial improvement would be to study the underwater volume of schools in relationship to the different school types observed from the plane. Indeed, the present approach assumes that the number of tunas is proportional to the school surface observed at the surface, but this has not been experimentally proven yet. Hyperspectral technologies provide interesting perspectives in that respect.

Environmental conditions are known to affect the spatial distribution of bluefin tuna in the GoL, through foraging in relationship to frontal structures and mixed layer depth (Royer *et al.*, 2005). This can translate into changes in the horizontal and vertical behaviour of EABFT in the GoL, affecting its detectability and availability to the survey (Bauer *et al.*, 2017). Such effects could be accounted for in the index of abundance, using suitable habitat approaches to derive the probability of occurrence in the survey area and at the surface, depending on environmental conditions (Druon *et al.*, 2011, 2016).

Acknowledgments

The authors thank pilots from previous aerial surveys for their help during data acquisition. Aerial surveys were funded by the European Union, through the project STROMBOLI (2000-2002, EU-DGXIV 99/022), the French Water Agency and the French Fisheries Administration.

References

Bauer, R. K., Bonhommeau, S., Brisset, B., and Fromentin, J. 2015. Aerial surveys to monitor bluefin tuna abundance and track efficiency of management measures. Marine Ecology Progress Series, 534: 221–234.

Bauer, R. K., Fromentin, J.-M., Demarcq, H., and Bonhommeau, S. 2017. Habitat use, vertical and horizontal behaviour of Atlantic bluefin tuna (*Thunnus thynnus*) in the Northwestern Mediterranean Sea in relation to oceanographic conditions. Deep Sea Research Part II: Topical Studies in Oceanography, 141: 248–261.

Bonhommeau, S., Farrugio, H., Poisson, F., and Fromentin, J.-M. 2010. Aerial surveys of bluefin tuna in the Western Mediterranean sea: retrospective, prospective, perspective. Collective Volume of Scientific Papers, 65: 801–811.

Buckland, S. T., Anderson, D. R., Burnham, K. P., and Laake, J. L. 2005. Distance Sampling. *In* Encyclopedia of Biostatistics. John Wiley & Sons, Ltd. http://onlinelibrary.wiley.com/doi/10.1002/0470011815.b2a16019/abstract (Accessed 1 March 2016).

Druon, J., Fromentin, J., Aulanier, F., and Heikkonen, J. 2011. Potential feeding and spawning habitats of Atlantic bluefin tuna in the Mediterranean Sea. Marine Ecology Progress Series, 439: 223–240.

Druon, J.-N., Fromentin, J.-M., Hanke, A. R., Arrizabalaga, H., Damalas, D., Tičina, V., Quílez-Badia, G., *et al.* 2016. Habitat suitability of the Atlantic bluefin tuna by size class: An ecological niche approach. Progress in Oceanography, 142: 30–46.

Fromentin, J.-M., Farrugio, H., Deflorio, M., and De Metrio, G. 2003. Preliminary results of aerial surveys of bluefin tuna in the western Mediterranean sea. Collective Volume of Scientific Papers, 55: 1019–1027.

Miller, D. L., Rexstad, E., Thomas, L., Marshall, L., and Laake, J. 2017. Distance Sampling in R. bioRxiv: 063891.

Rouyer, T., Brisset, B., Bonhommeau, S., and Fromentin, J.-M. 2018. Update of the abundance index for juvenile fish derived from aerial surveys of bluefin tuna in the western Mediterranean Sea. Collective Volume of Scientific Papers ICCAT, 74: 2887–2902.

Royer, F., Fromentin, J.-M., Farrugio, H., and Gaspar, P. 2005. Determining bluefin tuna habitat through frontal features in the Mediterranean Sea. Collective Volume of Scientific Papers ICCAT, 58: 1275–1284.

Thomas, L., Buckland, S. T., Burnham, K. P., Anderson, D. R., Laake, J. L., Borchers, D. L., and Strindberg, S. 2006. Distance Sampling. *In* Encyclopedia of Environmetrics. John Wiley & Sons, Ltd. http://onlinelibrary.wiley.com/doi/10.1002/9780470057339.vad033.pub2/abstract (Accessed 1 March 2016).

Table 1. Range of surface estimates, average of length estimate and sample size for the different school types.

School Type	*Surface min in m^2*	*Surface max in m^2*	*Average length in m*	*N*
Tiny	2	54	3	33
Small	9	743	10	13
Medium	627	1929	23	3
Large	59,490	73,536	132	2

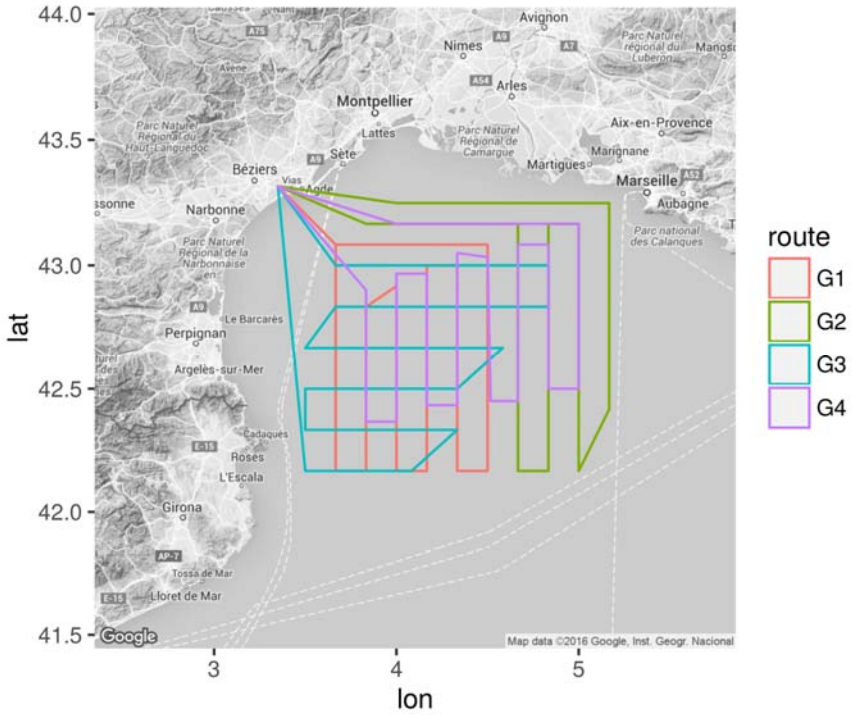

Figure 1. Maps of the different routes followed for the aerial surveys above the Gulf of Lions in the Northwestern Mediterranean.

Figure 2. Cessna pushpull 337, with the camera installed with the succion cup and the distance marks set-up on the wing arm.

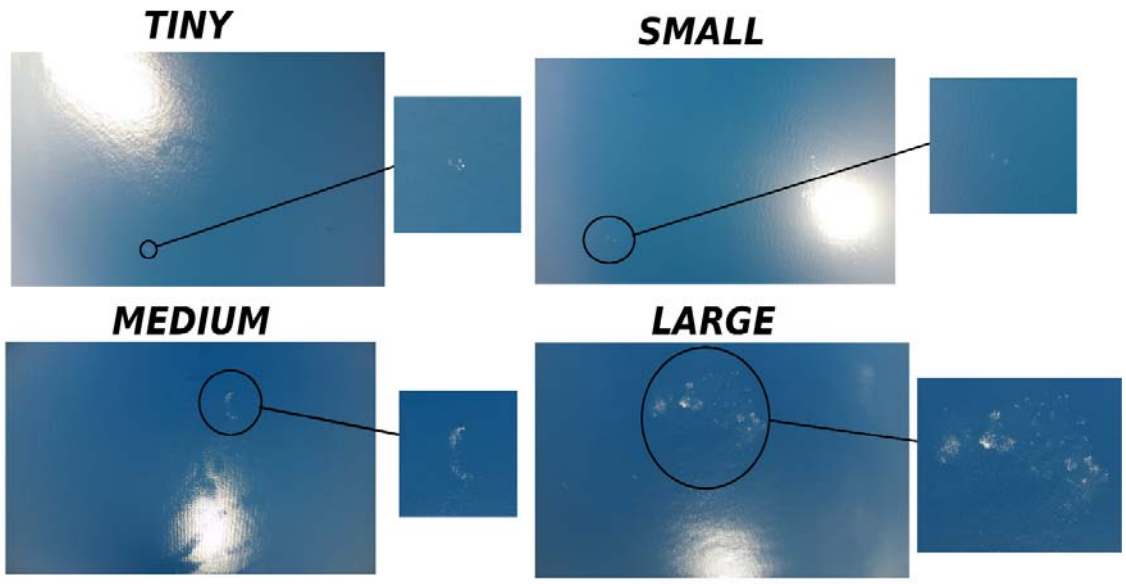

Figure 3. School types encountered during aerial surveys over the Gulf of Lions. The photos were obtained from videos shot by a GOPRO Hero 4 installed under the aircraft wing.

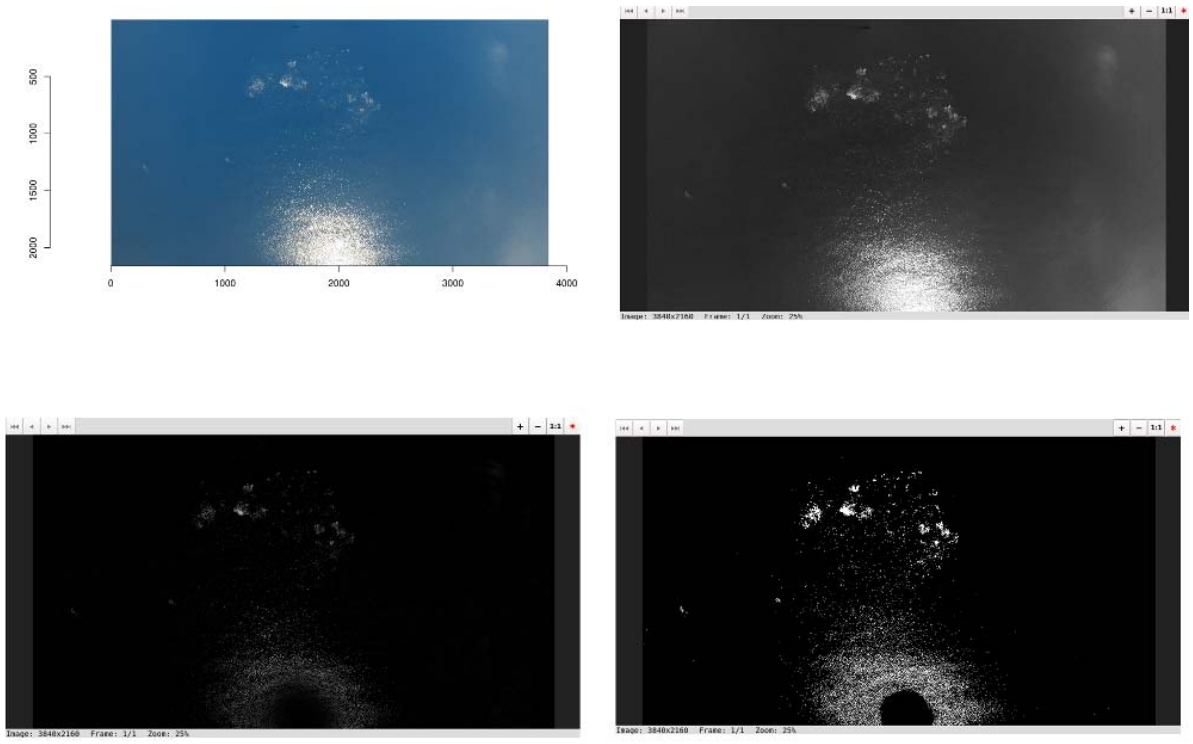

Figure 4. Different steps involved in the image processing for school surface estimation. Top Left, original image. Top Right, gray scaling. Bottom Left, substracting background. Bottom Right, thresholding.

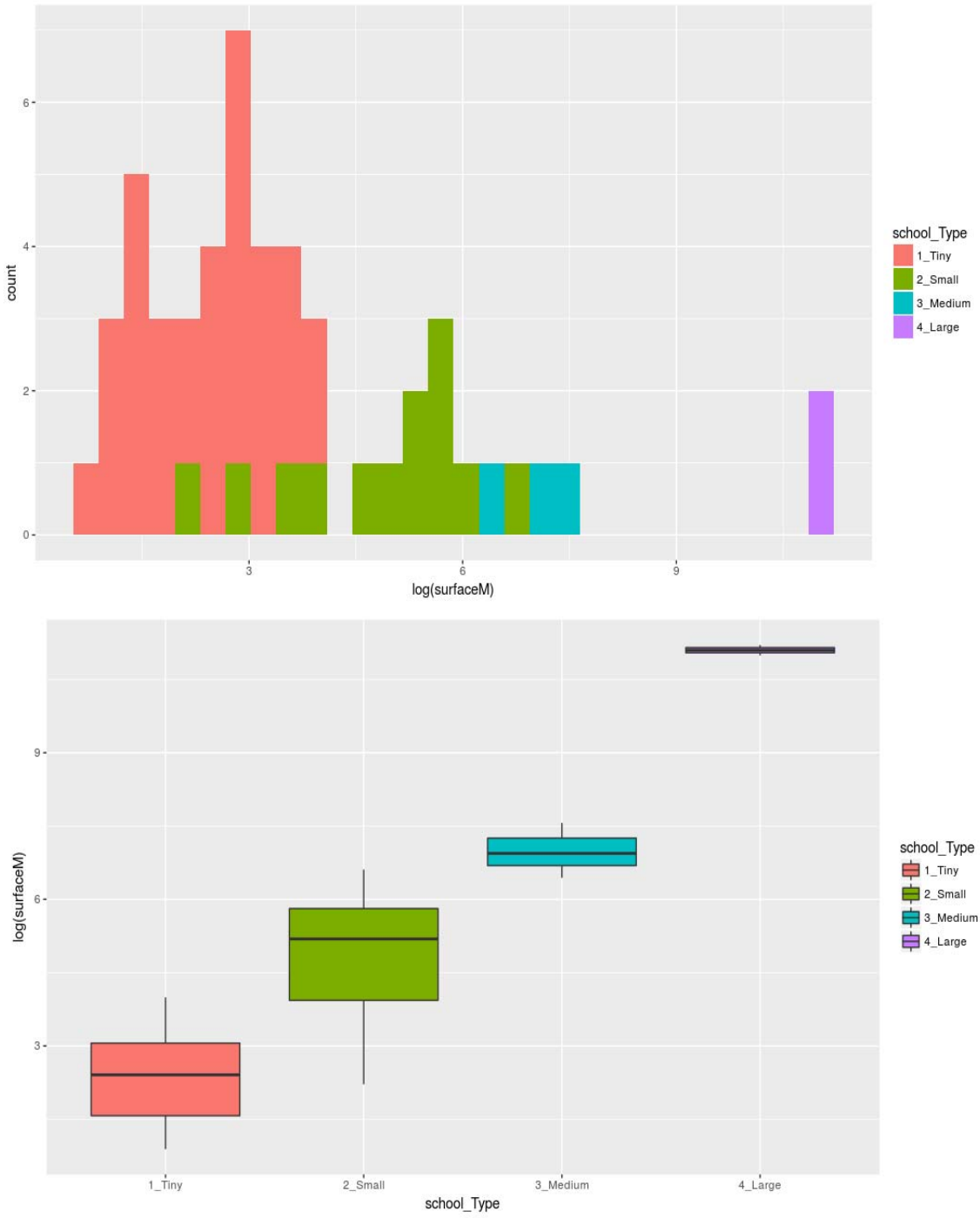

Figure 5. Histogram and boxplot of the log surfaces (in m^2) estimated for each school type.

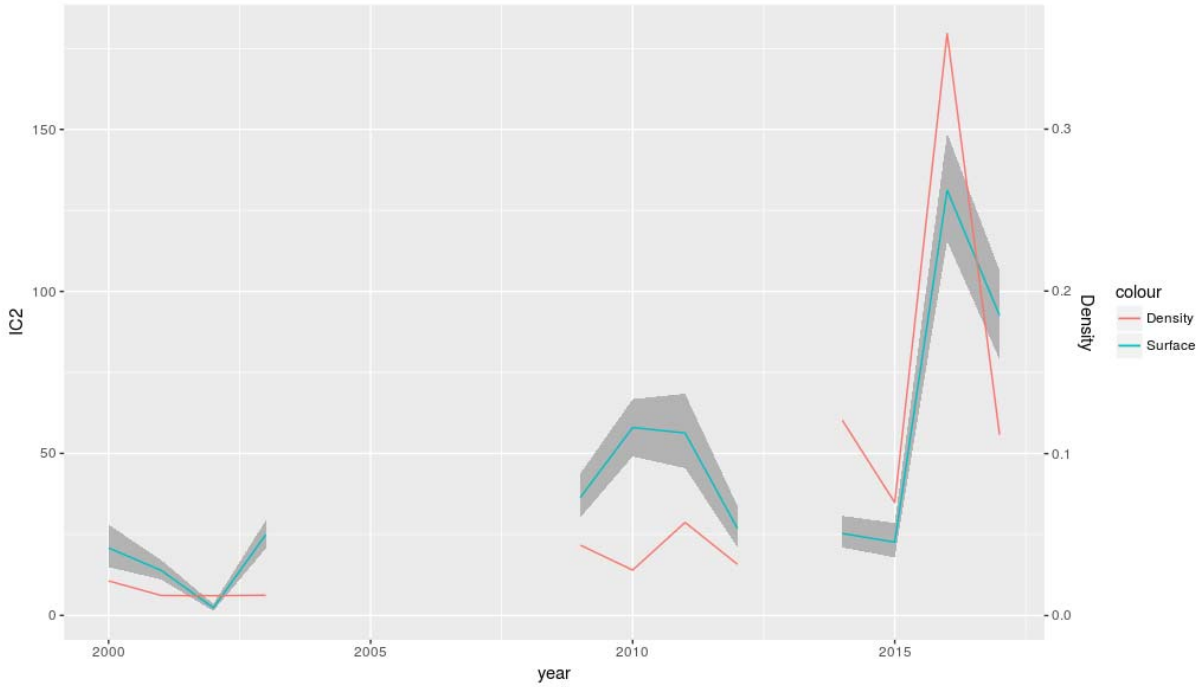

Figure 6. Index of abundance for 1000 bootstraps reflecting mis-attribution of school types and random attribution of school surface for each school type, and updated index for 2017. The latter refers to the inclusion of 2017 data to the 2000-2016 dataset and a re-run of the index using the same model specification than for the 2017 assessment.